

## Color of pure and alkali-doped cerium sulfide: A local-density-functional study

M.-A. Perrin

*Centre de Recherches de Rhône-Poulenc, 52 rue de la Haie Coq, 93308 Aubervilliers Cedex, France*

E. Wimmer

*Molecular Simulations, Parc Club Orsay Université, 20 rue Jean Rostand, 91893 Orsay, France*

(Received 23 February 1996)

The electronic structure and mechanisms for the optical excitations of pure and Na-doped  $\gamma$ -Ce<sub>2</sub>S<sub>3</sub> have been investigated using first-principles local-density-functional theory. The energy-band structures from augmented-spherical-wave calculations indicate that the S  $3p \rightarrow$  Ce  $5d$  interband transitions give rise to absorptions in the ultraviolet, whereas the observed red color of  $\gamma$ -Ce<sub>2</sub>S<sub>3</sub> is associated with localized Ce  $4f \rightarrow 5d$  excitations. The cationic vacancies in  $\gamma$ -Ce<sub>2</sub>S<sub>3</sub> (which is derived from the cubic Th<sub>3</sub>P<sub>4</sub> structure) lead to the formation of vacancy bands, which are split off from the top of the S  $3p$  valence band. Na doping removes these vacancy bands and homogenizes the band edges of the valence and conduction bands. As a consequence, the onset of the  $f \rightarrow d$  transitions is shifted slightly to larger energies and becomes sharper, which is consistent with an observed change in the color of  $\gamma$ -Ce<sub>2</sub>S<sub>3</sub> from maroon to red-orange upon doping with Na. [S0163-1829(96)05028-X]

### I. INTRODUCTION

At present, only few yellow and red pigments are available with high performance in their thermal, chemical, and uv stability. Cadmium sulfoselenide and compounds such as lead molybdate are currently the most widely used pigments of this kind. These compounds have excellent performance characteristics, but their toxicity is environmentally undesirable. Thus, driven by changes in legislation and government regulations, there is a strong incentive to develop new classes of inorganic pigments that are non-toxic and environmentally more compatible while preserving or even exceeding the optical, thermal, and chemical characteristics of present high-performance pigments.

To this end, rare-earth sulfides and related compounds have been proposed as promising candidates.<sup>1-3</sup> Within this class of compounds,  $\gamma$ -Ce<sub>2</sub>S<sub>3</sub> is particularly interesting since alkali doping makes it possible to tune its color from maroon to orange.<sup>2</sup> So far, progress in the development of these pigments has been mostly achieved by extensive synthetic efforts combined with physical characterization such as x-ray diffraction and optical measurements. Further systematic improvements are difficult without a detailed understanding of the relationships between the chemical composition, the crystallographic structure, and the optical properties of these compounds. Due to the complex crystal structure, the existence of vacancies, and the presence of  $f$  electrons, this understanding is still incomplete. In fact, even the fundamental mechanism causing the color of these compounds is not completely settled.

It is the aim of the present work to determine the electronic structure of cerium sulfide, to establish the role of the  $f$  electrons in the optical transitions, and to investigate the changes of the electronic structure induced by the doping with alkali atoms. As prototypical compounds we have chosen pure  $\gamma$ -Ce<sub>2</sub>S<sub>3</sub> and the alkali-doped compound Na<sub>0.5</sub>Ce<sub>2.5</sub>S<sub>4</sub>.<sup>2,3</sup> As reference we have also performed calcu-

lations on Ce<sub>3</sub>S<sub>4</sub>. The results show that the optical transitions in the visible spectrum can be understood by localized excitations from Ce  $4f$  levels into the conduction band of predominant Ce  $5d$  character while the interband transitions from the S  $3p$  valence band into the conduction band lead to absorptions above 3 eV in the uv range. The interband transitions can be directly interpreted from a one-particle band picture, while total-energy differences between ground and excited states of an atomic model are used to describe the localized excitations involving the  $f$  states. A rigid band model using the band structure of Ce<sub>3</sub>S<sub>4</sub> is insufficient to account for the details of the electronic structure of  $\gamma$ -Ce<sub>2</sub>S<sub>3</sub> because of the presence of vacancies. A major effect of sodium doping is the elimination of the vacancies and a homogenization of the band edges.

Rare-earth sesquisulfides have fascinating optical and magneto-optical properties and thus are the subject of a number of experimental studies. In the search for luminescence devices, Scharmer, Leiß, and Huber<sup>4</sup> investigated Ce- and Nd-doped lanthanum sulfides. For La<sub>2</sub>S<sub>3</sub>:Ce 1%:Nd 1% these authors attributed the fundamental absorption edge at 460 nm to a direct band gap at 2.6 eV and associated the broad absorptions centered at 540 and 470 nm with Ce  $4f \rightarrow 5d$  transitions. In a review of the optical properties and electronic structures of rare-earth sesquisulfides and sesquioxides, Zhuze and Shelykh<sup>5</sup> reported that the optical gaps of rare-earth sesquisulfides are between about 2.5 and 2.9 eV, with the exception of Ce<sub>2</sub>S<sub>3</sub>, for which a value of 2.2 eV is given. Furthermore, these authors discuss the potential role of the lanthanide  $f$  electrons in the chemical bonding. Gubanov and Ryzhkov<sup>6</sup> pointed out that at the beginning of the rare-earth series there could be a significant participation of the  $f$  electrons in the chemical bonding, which falls off with the stronger localization of the  $f$  levels for higher atomic numbers. This is consistent with the photoemission spectra of rare-earth sesquisulfides described by Kaciulis, Latisenka, and Plesanovas<sup>7</sup> who interpret a shoulder at about

2.5 eV (with respect to the Fermi level) in the photoemission spectrum of  $\text{Ce}_2\text{S}_3$  as originating from the Ce  $4f$  states. In the sesquisulfides of Nd, Sm, Gd, and Dy this spectral feature is shifted to 5.6, 8.0, 9.5, and 10.0 eV, respectively, and becomes an increasingly pronounced peak in the photoelectron spectrum. Kimura *et al.*<sup>8</sup> have measured the reflectivity spectrum of  $\text{Gd}_2\text{S}_3$  in the energy range from 2 meV to 30 eV and noted that the fundamental energy gap of this semiconductor does not vary with temperature and thus is thought to be due to direct transitions. This seems to contradict the band-structure results of Takegahara, Kaneta, and Kasuya,<sup>9</sup> who report an indirect gap for the isostructural  $\text{Th}_3\text{P}_4$ . As will be shown below, this result may not be directly relevant to the discussion of the rare-earth sesquisulfides. Recently, Dagys and Babonas<sup>10</sup> pointed out the special role of  $4f \rightarrow 5d$  transitions in  $\text{Ce}_2\text{S}_3$  to explain the optical and electrical characteristics. The fundamental optical transitions of typical  $\text{Ln}_2\text{O}_3$  and  $\text{Ln}_2\text{S}_3$  compounds are thought to involve O  $2p$  or S  $3p$  valence bands (Ln denotes lanthanide). Earlier, these authors had provided evidence from magneto-optical measurements that the absorption edge in  $\text{Ce}_2\text{S}_3$  at 2.2 eV may be related to  $4f \rightarrow 5d$  transitions and thus the absorption in this particular energy region is a unique feature due to cerium.<sup>11</sup> This interpretation is substantiated further by a study of the optical and magneto-optical properties of  $(\text{La}_{2-x}\text{Ce}_x)\text{S}_3$  crystals by Dagys, Babonas, and Pulinskas.<sup>12</sup> However, the accurate experimental assignment of optical gaps of rare-earth compounds is difficult, especially if only powders are available. Furthermore, the results are extremely sensitive to small impurities by other rare-earth elements and great caution has to be exercised in the assignment of optical gaps, unless the entire complex dielectric function on pure single crystals has been measured. In fact, very recent optical measurements by Witz *et al.*<sup>13</sup> on single crystals of  $\text{Ce}_2\text{S}_3$  and  $\text{Gd}_2\text{S}_3$  have revealed that the direct gap of the rare-earth sesquisulfides is larger than 3.3 eV, i.e., substantially higher than reported earlier by Zhuze and Shelykh.<sup>5</sup> For the mixed  $(\text{La}_{2-x}\text{Ce}_x)\text{S}_3$  Witz *et al.*<sup>13</sup> found a feature in the visible part of the spectrum at about 2.2 eV that depends directly on the Ce concentration and is absent for the pure La compound.

The first electronic-structure calculations for rare-earth sesquisulfides in the  $\text{Th}_3\text{P}_4$  structure have recently been reported by Mauricot *et al.*<sup>14</sup> These authors used a semiempirical extended Hückel approach to calculate the energy-band structure of  $\text{Ce}_3\text{S}_4$ . The results show a S  $3p$  valence band and a Ce  $5d$  conduction band. With their choice of semiempirical parameters, these authors obtain an indirect gap of about 2.5 eV, which is in the energy range reported by Zhuze and Shelykh.<sup>5</sup> The overall features of the energy-band structure resemble those of  $\text{Th}_3\text{P}_4$  as reported earlier by Suzuki *et al.*<sup>15</sup> In the calculations of Mauricot *et al.*<sup>14</sup> the  $4f$  electrons are not included. However, recent relativistic Hartree-Fock calculations on isolated Ce atoms and ions have been invoked by Dagys, Babonas, and Pukinskas<sup>12</sup> to probe the role of  $f \rightarrow d$  transitions.

While the importance of the  $4f$  levels in understanding the optical properties of rare-earth sulfides has thus been established, there is still a lack of a consistent theoretical approach that reconciles the band picture with the localized nature of the rare-earth  $f$  electrons to explain the optical spectra and color of rare-earth sesquisulfides. By choosing a

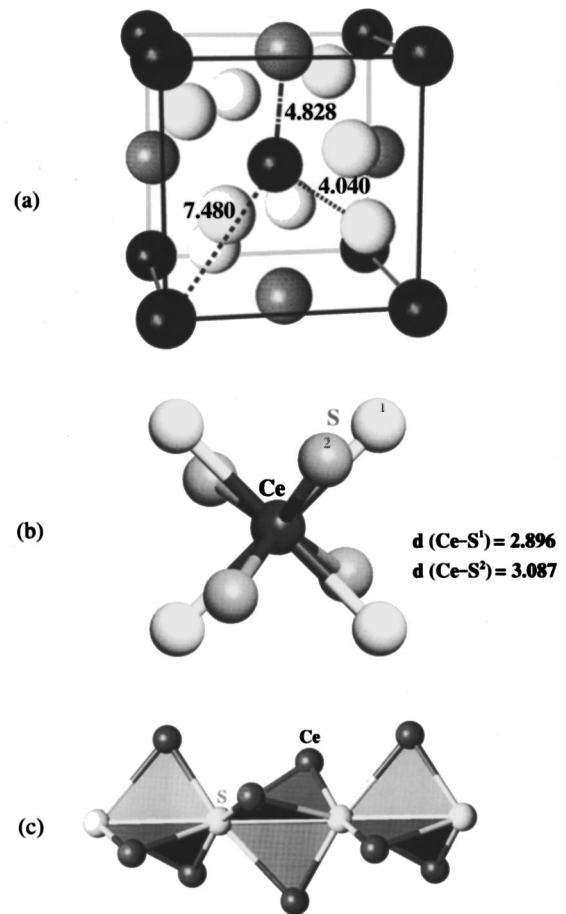


FIG. 1. Schematic representation of the  $\text{Th}_3\text{P}_4$  structure. The 12 cationic positions in the cubic unit cell are shown in (a). Note that there are three nearest-neighbor distances, which are marked in the figure in angstroms. (b) displays the eight nearest-neighbor anions around each cation with a local  $S_4$  symmetry. Note the two sets of Ce-S distances given in angstroms. (c) shows a motif with threefold symmetry along  $[111]$ , which reveals a distorted octahedral coordination of each sulfur atom.

local-density-functional approach and a combination of a band picture and total-energy differences within a localized atomic model, we demonstrate a first-principles approach that is free of the ambiguities of semiempirical and parametrized approaches, while still being computationally feasible for the systematic investigation of a range of different cases.

## II. STRUCTURAL MODELS AND COMPUTATIONAL APPROACH

The parent structure of pure and alkali-doped  $\gamma\text{-Ce}_2\text{S}_3$  is  $\text{Th}_3\text{P}_4$ , which crystallizes in the cubic space group  $I\bar{4}3d$ .<sup>16</sup> In a recent systematic study by Mauricot *et al.*,<sup>14</sup> the details of the crystallographic structure of pure and alkali-doped rare-earth sulfides have been mapped out. These experimental structural results are used in the present calculations.

In the  $\text{Th}_3\text{P}_4$  structure the cations form a body-centered-cubic lattice with 12 cationic sites per unit cell [cf. Fig. 1(a)]. All of these 12 sites are symmetry equivalent with a local  $S_4$  point-group symmetry [cf. Fig. 1(b)]. Each cation is sur-

rounded by eight anions, as shown in Fig. 1(b), with two different nearest-neighbor distances. In the case of  $\text{Ce}_3\text{S}_4$  these distances are 2.896 and 3.087 Å, respectively. Along the [111] direction, S-Ce-S chains form a motif with three-fold symmetry, as shown in Fig. 1(c), revealing a distorted octahedral coordination of the anions. The conventional cubic unit cell of  $\text{Ce}_3\text{S}_4$  contains 28 atoms and thus can be written as  $\text{Ce}_{12}\text{S}_{16}$ .

The structure of  $\gamma\text{-Ce}_2\text{S}_3$  is formally derived from  $\text{Ce}_3\text{S}_4$  by removing one out of nine Ce atoms from the lattice. With reference to the conventional unit cell,  $\gamma\text{-Ce}_2\text{S}_3$  can thus be written as  $(V_{\text{Ce}})_{1/3}\text{Ce}_{10/3}\text{S}_{16}$  with  $V_{\text{Ce}}$  indicating a vacancy on the Ce sublattice. Obviously, one would need to triple the conventional cubic unit cell of the  $\text{Th}_3\text{P}_4$  structure to accommodate the stoichiometry of  $\gamma\text{-Ce}_2\text{S}_3$ . The vacancies are randomly distributed<sup>14</sup> and thus one can expect a statistical occurrence of different environments around each vacancy. This can be rationalized by writing

$$(V_{\text{Ce}})_{1/3}\text{Ce}_{10/3}\text{S}_{16} = \frac{1}{3}\{2V_{\text{Ce}}\text{Ce}_{11}\text{S}_{16} + (V_{\text{Ce}})_2\text{Ce}_{10}\text{S}_{16}\}. \quad (1)$$

If one uses the conventional cubic unit cell as reference (cf. Fig. 1), there is only one possibility to form  $V_{\text{Ce}}\text{Ce}_{11}\text{S}_{16}$ , i.e., to introduce a single vacancy, since all Ce atoms in  $\text{Ce}_{12}\text{S}_{16}$  are equivalent. Statistically, the arrangement with a single vacancy carries twice the weight of the situation  $(V_{\text{Ce}})_2\text{Ce}_{10}\text{S}_{16}$ , which represents two vacancies per unit cell.

Upon doping of  $\gamma\text{-Ce}_2\text{S}_3$  with sodium, all vacancies are filled with Na atoms and 1 out of 16 Ce atoms is replaced by an alkali atom. This results in a stoichiometry of  $\text{Na}_2\text{Ce}_{10}\text{S}_{16}$  or  $\text{Na}_{0.5}\text{Ce}_{2.5}\text{S}_4$ . Geometrically, this is equivalent to the vacancy structure  $(V_{\text{Ce}})_2\text{Ce}_{10}\text{S}_{16}$  discussed previously. Substitution of two Ce atoms in the cubic unit cell leads to three possibilities that correspond to replacing the central atom of the cubic unit cell by a vacancy or a Na atom and then substituting the first, second, or third nearest cation at 4.040, 4.828, or 7.480 Å, respectively [cf. Fig. 1(a)]. Calculations have been performed for all of these possibilities.  $\text{Na}^+$  and  $\text{Ce}^{3+}$  have similar ionic radii (1.07 and 0.98 Å, respectively), hence the same anionic environment is assumed for the cerium and sodium atoms consistent with the x-ray-diffraction study by Mauricot *et al.*<sup>14</sup> The structural data used for the present calculations are summarized in Table I. For  $\text{Ce}_3\text{S}_4$  we have used the same relative sulfur positions (described by the parameter  $u$ ) as obtained from the recent crystallographic measurements<sup>14</sup> on  $\gamma\text{-Ce}_2\text{S}_3$  and  $\text{Na}_{0.5}\text{Ce}_{2.5}\text{S}_4$  rather than the old values given by Zachariassen.<sup>16</sup> However, as a check we have also performed the calculations on  $\text{Ce}_3\text{S}_4$  with the original parameters given by Zachariassen.<sup>16</sup> A change of the lattice constant from 8.623 to 8.635 Å has no noticeable effect on the energy-band structure, whereas a slight difference can be seen between the cases  $u=0.083$  (from Zachariassen<sup>16</sup>) and  $u=0.0725$  (after Mauricot *et al.*<sup>14</sup>). These differences are small compared to the changes induced by the vacancies. It should be noted that the compounds  $\gamma\text{-Ce}_2\text{S}_3$  and  $\gamma\text{-Na}_{0.5}\text{Ce}_{2.5}\text{S}_4$  are semiconductors, whereas  $\text{Ce}_3\text{S}_4$  is metallic.<sup>17</sup> However, the issue of electrical conductivity of cerium sulfides is outside the scope of the present paper and will not be further discussed here.

TABLE I. Lattice parameters  $a_0$  and crystallographic parameter  $u$  defining the positions of the S atoms used in the present calculations. All structures are derived from the cubic  $\text{Th}_3\text{P}_4$  structure of space group  $I43d$ . The symbol  $V_{\text{Ce}}$  denotes vacancies on the cationic sites as explained in the text. A detailed discussion of the crystallography of this structure is given in Refs. 14 and 16.

Compound	$a_0$ (Å)	$u$
$\text{Ce}_3\text{S}_4^a$	8.623	0.083
$\text{Ce}_6\text{S}_4^b$	8.635	0.0731
$\gamma\text{-Ce}_2\text{S}_3^c$	8.631	0.0731
$\text{Na}_2\text{Ce}_{10}\text{S}_{16}^c$	8.6371	0.0725
$V_{\text{Ce}}\text{Ce}_{11}\text{S}_{16}, (V_{\text{Ce}})_2\text{Ce}_{10}\text{S}_{16}, \text{Na}_2\text{Ce}_{10}\text{S}_{16}^b$	8.6371	0.0725

<sup>a</sup>Reference 16.

<sup>b</sup>Present work.

<sup>c</sup>Reference 14.

The present electronic-structure calculations are based on density-functional theory with the local-density approximation (LDA).<sup>18</sup> This method is well known to give a good description of the structural and electronic properties of a wide range of solids including rare-earth compounds with 4f electrons.<sup>19–24</sup> However, one has to be careful in distinguishing between the fundamental quantities of density-functional theory, namely, the total electron density and the total energy and auxiliary quantities such as one-particle eigenvalues (i.e., energy-band structures and densities of states), as will be discussed below. Spin polarization and magnetic effects, while fascinating and important in their own right, are not critical in the understanding of the purely optical properties of Ce sulfides. For this reason, all calculations reported here are non-spin-polarized.

We use the form of Hedin and Lundqvist<sup>25</sup> for the local exchange and correlation terms. The effective one-particle Schrödinger equations of Kohn-Sham theory are solved with the augmented-spherical-wave (ASW) method<sup>26</sup> as implemented in the ESOCS computer program.<sup>27</sup> Relativistic effects are included in a semirelativistic approximation as given by Koelling and Harmon.<sup>28</sup> The Ce 4f electrons are treated as valence states. The ASW method, which is similar to the linearized muffin-tin orbital method of Andersen,<sup>29</sup> uses the atomic sphere approximation (ASA). In the ASA, the entire space of the unit cell is spanned by overlapping atomic spheres with a spherically symmetric potential in each atomic sphere. The fairly dense  $\text{Th}_3\text{P}_4$  structure lends itself well to this approximation. With the choice of atomic sphere radii as given in Table II the overlap between the spheres is less than 13% of the total cell volume. The energy-band-structure calculations that capture the itinerant aspects of the electronic structure are complemented by fully relativistic density-functional calculations on an isolated Ce atom in order to understand intra-atomic excitations involving the f electrons.<sup>30</sup>

### III. RESULTS AND DISCUSSION

Figure 2 shows the LDA energy-band structures of  $\text{Ce}_{12}\text{S}_{16}$  (i.e.,  $\text{Ce}_3\text{S}_4$ ) and the vacancy structures  $V_{\text{Ce}}\text{Ce}_{11}\text{S}_{16}$  and  $(V_{\text{Ce}})_2\text{Ce}_{10}\text{S}_{16}$  that are models of  $\gamma\text{-Ce}_2\text{S}_3$ . The most striking feature in all the band structures is a narrow set of

TABLE II. Atomic-sphere radii used in the present augmented-spherical-wave calculations with the ESOCS program (Ref. 27). The relative overlap, i.e., the sum of the overlap between the atomic spheres relative to the volume of the unit cell, is 12.4%. The number of  $k$  points is determined by a constant real-space cutoff, which leads to eight  $k$  points in the irreducible part of the first Brillouin zone.

Compounds/Atoms	$R_{ASA}$ (Å)
$Ce_3S_4$	
Ce	1.895 76
S	1.650 59
$V_{Ce}Ce_{11}S_{16}$ , $(V_{Ce})_2Ce_{10}S_{16}$ , $Na_2Ce_{10}S_{16}$	
Ce, $V_{Ce}$ , Na	1.896 48
S	1.650 74

bands with a width of about 0.8 eV that originates from the Ce 4*f* states. Because of their treatment as valence states, these “*f* bands” are pinned to the Fermi level. Near the bottom of the *f* bands one finds a noticeable dispersion, especially near the point  $\Gamma$  [cf. Fig. 2(a)]. This dispersion is less pronounced in the cases in which the conduction bands, which have predominantly Ce 5*d* character, are more separated from the *f* bands [cf. Figs. 2(b)–2(e)]. This hybridization between *f* bands and conduction bands indicates some participation of the *f* states in the chemical bonding as suggested by Gubanov and Ryzhkov.<sup>6</sup> The valence bands below the *f* bands have predominantly S 3*p* character. For  $Ce_3S_4$ , in which all cationic sites are occupied with Ce atoms, the band gap between the valence and conduction bands is direct and the LDA value is 3.1 eV.

The energy-band structures for the cerium sulfides with

vacancies on the cationic sublattice are shown in Figs. 2(b)–2(e). The overall features of these band structures are similar to that of  $Ce_3S_4$ , but two important differences are evident [cf. Figs. 2(a) and 2(b)–2(e)]: (i) The energy of the top of the valence bands depends strongly on the presence of vacancies and (ii) the vacancies in the Ce sublattice give rise to “vacancy bands” that are split off from the top of the S 3*p* valence bands. As a consequence, the fundamental gap between the valence and the conduction band diminishes substantially with increasing vacancy concentration. In the case of a single vacancy [Fig. 2(b)] and in the structure with two vacancies separated by 7.480 Å [Fig. 2(c)], vacancy bands are found slightly above the top of the valence bands. These bands originate from S *p* states that have dangling bonds into the vacancy. Because of the lack of an attractive cation, the one-particle energy of these states is higher than those of the other S *p* states. The vacancy bands are fairly flat except near  $\Gamma$ , where the bands show a weak upward dispersion. In the cases of a closer proximity of the vacancies, namely, 4.828 Å [Fig. 2(d)] and 4.040 Å [Fig. 2(e)], the vacancy bands are split into several distinct bands due to interactions between the vacancy states. Close proximity of the vacancies also causes the bands to be shifted even further away from the top of the valence bands towards smaller binding energies. Interestingly, in the case of the nearest possible distance between the vacancies of 4.040 Å [Fig. 2(e)], the maximum of the vacancy band is no longer at  $\Gamma$ , which would imply that the lowest transition from this occupied band into the conduction band would be indirect. However, since the vacancies in the real crystal are presumably statistically distributed,<sup>14</sup> the translational symmetry is broken and the concept of direct vs indirect band gaps loses its meaning.

Depending on the concentration and distribution of the

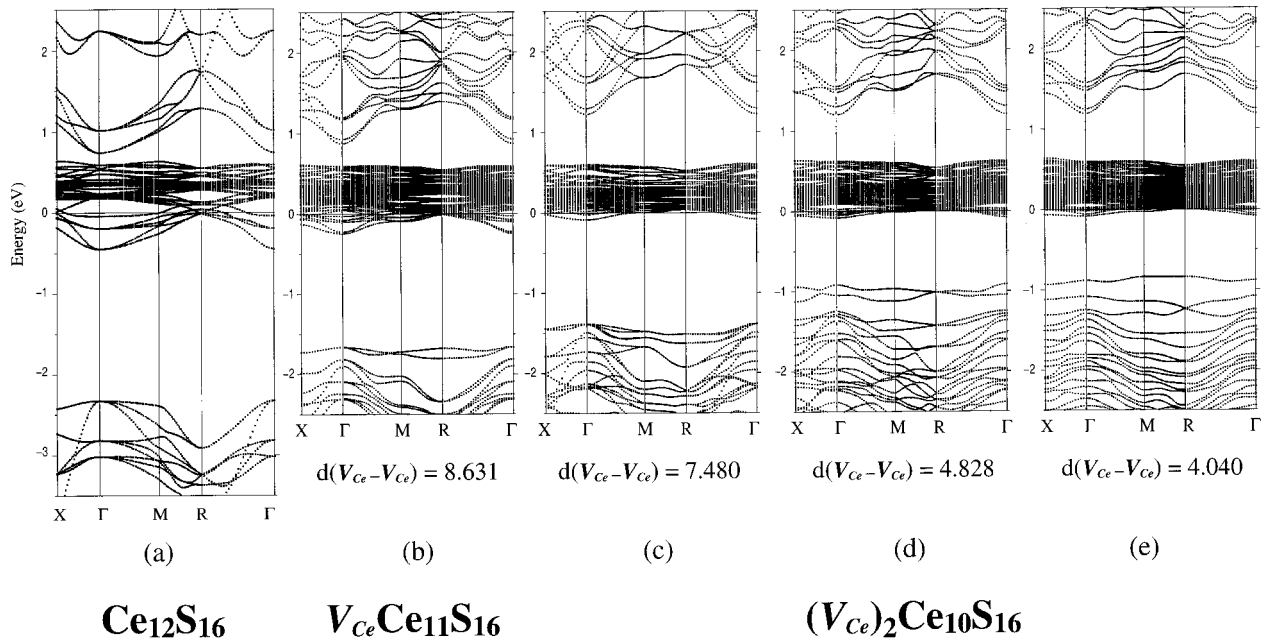
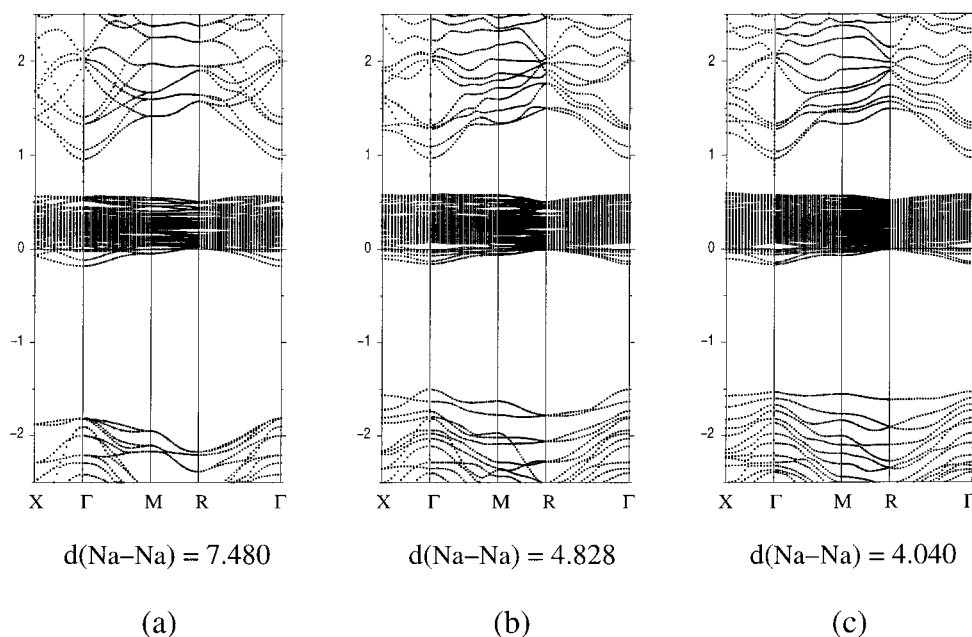


FIG. 2. Characteristic parts of the energy-band structures as obtained from local-density-functional augmented-spherical-wave calculations within the atomic-sphere approximation for (a)  $\gamma$ - $Ce_3S_4$ , (b)  $V_{Ce}Ce_{11}S_{16}$ , and (c)–(e)  $(V_{Ce})_2Ce_{10}S_{16}$  in three different arrangements of vacancy pairs corresponding to the three nearest-neighbor distances between cationic sites shown in Fig. 1. For ease of comparison, all energy band structures are shown for  $k$  points that correspond to a simple cubic structure.



## Na<sub>2</sub>Ce<sub>10</sub>S<sub>16</sub>

FIG. 3. LDA ASW-ASA energy-band structures for  $\gamma$ -Na<sub>2</sub>Ce<sub>10</sub>S<sub>16</sub> in three different arrangements of the Na atoms corresponding to the three cationic distances shown in Fig. 1.

vacancies, the LDA band gap varies between 2.07 eV (two vacancies in close proximity) and 2.62 eV. This constitutes a substantial reduction compared with the LDA gap of 3.1 eV for the vacancy-free Ce<sub>3</sub>S<sub>4</sub> structure. For the interpretation of the interband transitions in  $\gamma$ -Ce<sub>2</sub>S<sub>3</sub> one has to take into account the statistical distribution of the vacancies. From the periodic models shown in Fig. 2 one deduces a LDA energy difference between the highest valence states and the lowest conduction states of about 2.1–2.6 eV. The smallest energy difference, namely, 2.1 eV, comes from the case where two cationic vacancies are in the closest proximity [cf. Fig. 2(e)]. In  $\gamma$ -Ce<sub>2</sub>S<sub>3</sub> with disordered vacancies this arrangement of vacancies is likely to occur. Thus the LDA gap of 2.1 eV represents a lower limit for transitions between the valence and conduction bands. (In this model, lifetime broadening effects due to the lack of translational symmetry of the vacancies in a real crystal are not included.)

It is well known that the LDA band gap is typically smaller by a factor of about 0.6 compared to the experimental value. With a LDA value of 2.1 eV as the lower limit for the band gap, one would predict an experimental gap of 3.5 eV. The recently determined band gap of about 3.5 eV for the interband transitions in cerium sulfide crystals<sup>13</sup> would thus be perfectly consistent with the calculated LDA energies. The initial states of the interband transitions with the lowest excitation energies would involve mainly vacancy states. Due to the statistical distribution of the vacancies and the significant dependence of the gap energy on the local environment of the vacancy, these transitions would not have a very clear edge. At higher energies, the transitions would start from itinerant S 3*p* states and thus would resemble the direct interband transitions of perfectly ordered semiconductors with a direct band gap. Obviously, a rigid band model

using the energy bands of the fully occupied Ce<sub>3</sub>S<sub>4</sub> structure is inadequate to describe the surprisingly large changes caused by the vacancies on the cationic sublattice.

In a second set of calculations, all cationic vacancies as well as some Ce sites of the previous cases are occupied with Na atoms, as explained in Sec. II [cf. Figs. 3(a)–3(c)]. For Na<sub>2</sub>Ce<sub>10</sub>S<sub>16</sub> the overall features of the energy-band structures are very similar to the vacancy structures shown in Figs. 2(c) and 2(d). The major effect of Na doping is a stabilization of the S *p* states relative to the Ce 4*f* and the conduction bands. This stabilization is plausible since in the alkali-doped compounds each S atom is on average surrounded by more positive charges compared to the vacancy structure. This makes the electronic potential for the S states more attractive and shifts the valence bands to lower energies. In the Na-doped structures one can see the remnants of the vacancy bands [see, for example, Figs. 2(d) and 3(b)]. These states, however, now have Na *s* character and are closer to the top of the valence band compared to the vacancy bands of the pure sulfides. Na doping homogenizes the valence and conduction bands in the sense that the variations in the band gaps, which depend on the distribution of the vacancies [cf. Figs. 2(b)–2(e)], are less pronounced. As a consequence, the gap of the interband transitions is predicted to increase by about 0.4 eV upon doping of  $\gamma$ -Ce<sub>2</sub>S<sub>3</sub> with Na.

As stated earlier, the local character of excitations involving the Ce *f* states requires special attention and it can be misleading to refer to a “position” of the *f* bands for the following reason. If one considers a free Ce atom (cf. Fig. 4) and one carries out self-consistent relativistic local-density-functional calculations for different occupations of the *f* states, one finds that the Kohn-Sham functional is minimized for an effective occupation of 1.56 for the *f* states (provided

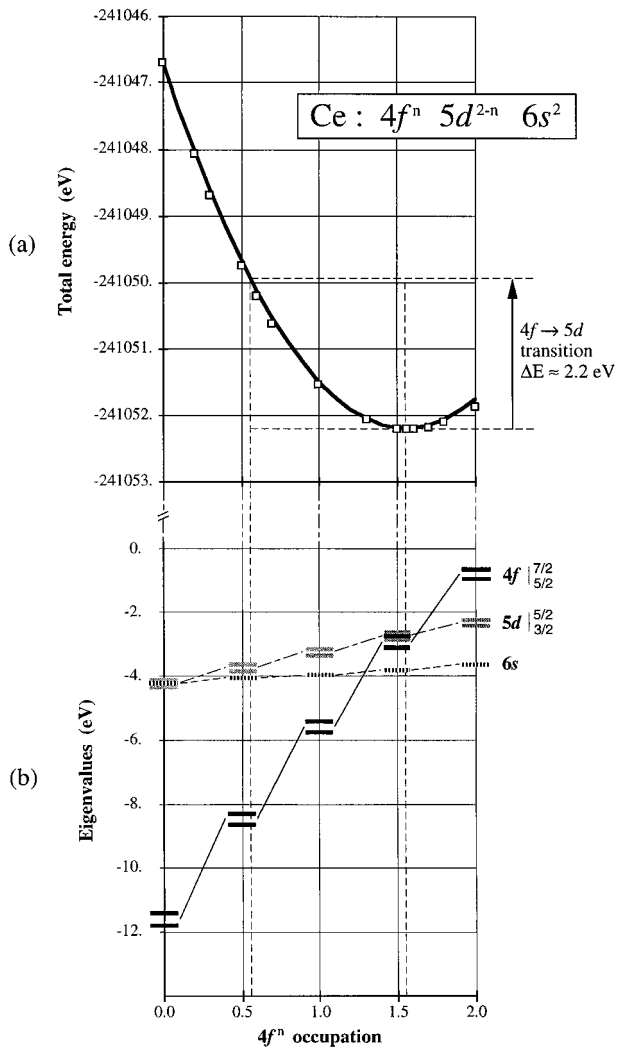


FIG. 4. The upper panel shows the total energy of an isolated neutral Ce atom as a function of the  $4f$  occupation as obtained from relativistic numerical atomic calculations. The minimum of the total energy corresponds to an  $f$  occupation of about 1.56. The change in the total energy upon promotion of one  $f$  electron into a  $5d$  state amounts to about 2.2 eV and is interpreted as the basic mechanics for the optical absorption in the visible part of the spectrum. The lower panel shows the local-density-functional one-particle eigenvalues. It can be seen that the  $4f$  one-particle energy depends dramatically on the occupation of this level. Upon the  $f \rightarrow d$  promotion the  $4f$  one-particle eigenvalue drops by more than 5 eV, whereas the total energy changes only by about 2 eV. The spin-orbit splitting of the  $f$  and  $d$  levels is indicated on scale, showing that spin-orbit effects are fairly small.

that one accepts fractional occupations of atomic states). Interestingly, this number of about 1.5  $f$  electrons in the ground state of Ce is also found from the energy-band-structure calculations on the cerium sulfides when the  $f$  states are treated as bands. The promotion of one  $f$  electron into a  $d$  state causes a change of the total energy by about 2.2 eV and one can refer to this excitation mechanism as an  $f \rightarrow d$  transition. Note that the one-particle eigenvalues for

the ground state of the Ce atom (cf. Fig. 4) do not permit such an interpretation directly. In fact, the one-particle energy of the Ce  $4f$  levels varies dramatically with the occupation. For example, the removal of one  $f$  electron causes the one-particle eigenvalue to drop by more than 5 eV. In contrast, the Ce  $5d$  states exhibit a much weaker dependence of the one-particle energies on the occupation. One could also use Slater's transition state concept<sup>31</sup> and approximate the total-energy difference of the  $f \rightarrow d$  transition by a calculation with half an electron in the initial state and half an electron in the final state. In that case, the  $4f$  occupation would be 1.06 and the difference between the  $4f$  and  $5d$  states (as a difference between one-particle energies) would be about 2.2 eV (cf. Fig. 4), which is equal to the total-energy differences.

It is reasonable to assume that the atomic character of the Ce  $4f$  electrons is similar in a free Ce atom and a Ce atom in the sulfide because of the localized nature of the  $4f$  states (the radial expectation value of the Ce  $4f$  functions is about 0.6 Å). In contrast, the Ce  $5d$  functions are much more extended (in the free atom they have a radial expectation value of about 1.7 Å) and are more strongly influenced by the chemical environment in the condensed phase. Therefore, the agreement between the value of 2.2 eV obtained for the  $f \rightarrow d$  transition from a model calculation on an isolated atom and the experimental absorption of cerium sulfide at exactly that energy is probably fortuitous.

In order to check the sensitivity of the energy of this  $f \rightarrow d$  transition on the chemical environment of Ce, we have carried out further model calculations for a substantially modified effective potential as shown in Fig. 5. To this end, we have added the following artificial external potential to the atomic Ce potential:

$$V_{\text{ext}}(r) = V_s \frac{1}{e^{(r-r_0)/\beta} + 1}, \quad (2)$$

with  $V_s = -10$  eV,  $r_0 = 1.5$  Å, and  $\beta = 0.2$  Å. This amounts to a shift by  $-10$  eV of the effective potential in the inner region of the Ce atom and no shift in the outer region with a Fermi function providing a smoothness throughout the entire radial region. The self-consistent calculations for the Ce atom with occupations  $f^{1.56}d^{0.44}$  and  $f^{0.56}d^{1.44}$  lead to a total-energy difference for the  $f \rightarrow d$  transition of 3.6 eV compared to 2.2 eV for the unperturbed Ce atom. This sensitivity check shows that even with a fairly strong perturbation of the effective potential of the Ce atom, the energy of the localized  $f \rightarrow d$  transition remains within the visible part of the electromagnetic spectrum. Thus the orange-red color of cerium sulfides can be explained by excitoniclike transitions involving the promotion of a localized Ce  $4f$  electron into states of the conduction band with predominantly Ce  $5d$  character. As can be seen from Fig. 5, the changes in the total-energy differences are reflected in the relative separation of the one-particle eigenvalues. In fact, for the unperturbed Ce atom in the ground state, the eigenvalues of the  $4f$  and  $5d$  states are almost the same, whereas for the perturbed case the  $5d$  states are about 1.8 eV higher than the  $4f$  states. Keeping this correspondence in mind, the position of the bottom of the Ce  $5d$  conduction band with respect to the bottom of the Ce  $4f$

bands provides a relative measure (but not an absolute value) for the excitation energy of the localized  $f \rightarrow d$  transition.

The influence of alkali doping on the energy-band structure and consequently on the color of cerium sulfide pigments can be seen from a comparison between the energy-band structures of the vacancy structures  $V_{\text{Ce}}\text{Ce}_{11}\text{S}_{16}$ ,  $(V_{\text{Ce}})_2\text{Ce}_{10}\text{S}_{16}$ , and the Na-doped cerium sulfide pigment  $\text{Na}_2\text{Ce}_{10}\text{S}_{16}$  (cf. Figs. 2 and 3). Na doping homogenizes the energies of the final state in the following way. In the undoped  $\text{Ce}_2\text{S}_3$  one can assume a statistical distribution of the vacancies with domains resembling the situation described by a single vacancy [cf. Fig. 2(b)] and by two vacancies [Figs. 2(c)–2(e)]. In the Fig. 2(b), which is statistically predominant, the bottom of the conduction band is located at about 0.8 eV and in the Figs. 2(c)–2(e) it is at about 1.2 eV above the Fermi level. The lowest  $f \rightarrow d$  transitions would thus be spread over a range of at least 0.4 eV. Na doping brings the bottom of the conduction band uniformly to about 0.9 eV, thereby creating a sharper edge in the absorption spectrum and shifting the lowest possible transition slightly towards higher energies, i.e., shorter wavelength. This would be consistent with an observed shift<sup>32</sup> in the color of  $\gamma\text{-Ce}_2\text{S}_3$  from maroon to red-orange upon doping with Na. The effect of alkali doping on the  $f \rightarrow d$  transitions is indirect because the wave functions involved in the transition are predominantly localized on specific Ce atoms, which are separated from the vacancies or alkali dopants by sulfur atoms. Consequently, the influence is very subtle and close to the relative accuracy of the present theoretical and computational approach.

#### IV. SUMMARY AND CONCLUSION

In this study we have shown that the electronic mechanism that controls the key optical properties of inorganic pigments such as alkali-doped cerium sulfides can be explained by first-principles local-density-functional calculations. The major results of the present investigation can be summarized as follows.

(i) The color of pure and alkali-doped  $\gamma\text{-Ce}_2\text{S}_3$  has its electronic origin in localized  $f \rightarrow d$  transitions, which are excitoniclike transitions from Ce  $4f$  states into the conduction band of predominantly Ce  $5d$  character. A theoretical description of these excitations is given by calculations of total-energy differences within a localized atomic model. Solid-state effects influencing the energies of these transitions are obtained from band-structure calculations by analyzing the energy difference between the Ce  $4f$  bands and the Ce  $5d$  conduction bands.

(ii) The interband transitions from the S  $3p$  valence bands into the Ce  $5d$  conduction bands lead to absorptions in the ultraviolet. For  $\gamma\text{-Ce}_2\text{S}_3$  these transitions are at wavelengths shorter than about 350 nm.

(iii) The presence and geometric arrangement of vacancies on the cationic sublattice in  $\gamma\text{-Ce}_2\text{S}_3$  have a strong influence on the size of the gap between the valence and conduction bands. In particular, the presence of two adjacent cationic vacancies can reduce the band gap by about 1 eV compared to the vacancy-free  $\text{Ce}_3\text{S}_4$  structure. (Thus a rigid band model based on the band structure or density of states

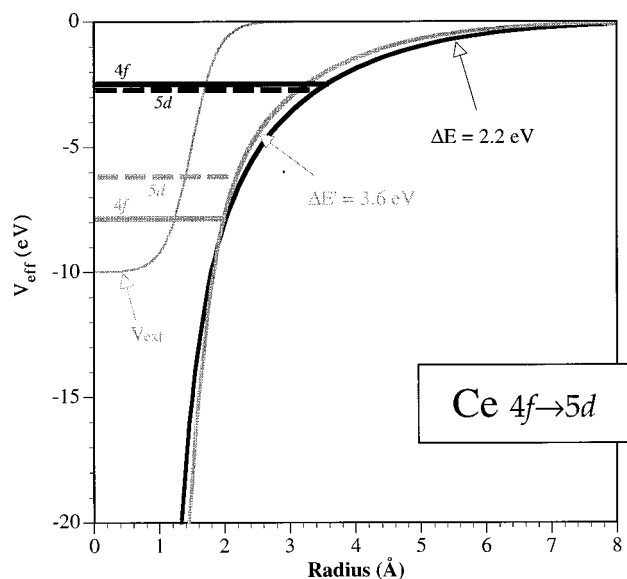


FIG. 5. Effective potential (in eV) of an unperturbed Ce atom (solid black line) and a perturbed potential as described in the text (solid gray line).  $V_{\text{ext}}$  denotes the external potential used to perturb the system. Total-energy differences related to the  $f \rightarrow d$  promotion are denoted by  $\Delta E$  and  $\Delta E'$  for the unperturbed and perturbed systems, respectively. The one-particle eigenvalues for the  $4f$  and  $5d$  states are drawn as horizontal lines. For clarity, only the  $j$ -average is shown and not the spin-orbit splitting. Note that the change of the total-energy differences is reflected in the relative displacement of the one-particle eigenvalues.

of  $\text{Ce}_3\text{S}_4$  in the perfect  $\text{Th}_3\text{P}_4$  structure would be inadequate for a quantitative description of  $\gamma\text{-Ce}_2\text{S}_3$ .)

(iv) The doping of  $\gamma\text{-Ce}_2\text{S}_3$  with alkali metals homogenizes the band edges by suppressing the vacancy bands and the variations in the band gap due to different vacancy distributions. As a consequence, it is predicted that upon Na doping of  $\gamma\text{-Ce}_2\text{S}_3$ , the interband transitions are shifted to larger energies by about 0.4 eV. The effect is indirect and is mediated by the S  $3p$  component of the conduction bands (which are predominantly of Ce  $5d$  character). The electronic origin of this shift is the energetic stabilization of the S  $3p$  levels when the vacancies are filled with electropositive atoms such as Na.

In contrast to compound semiconductors such as CdS and CdSe, where the color is controlled by interband transitions, the transitions from the anionic valence band into the cationic conduction band in cerium sulfides occur in the ultraviolet and the color of cerium-based pigments is explained in terms of atomiclike  $f \rightarrow d$  transitions. In other words, the color is largely an intrinsic property of cerium rather than a band-structure effect.

Based on the methodology presented in this study, it seems to be possible to use first-principles density-functional theory within the local-density approximation to predict the color of novel compounds or at least to point to the key electronic features that determine the optical transitions in the visible and ultraviolet parts of the spectrum. If this approach is to be used as a quantitative predictive tool, then three major issues still have to be settled: (i) one has to be able to predict the structural and thermodynamic stability of

a newly proposed compound, in principle, by exploring all possible crystal structures; (ii) absolute values for transition energies need to be calculated, which requires explicit approaches to excitation energies, possibly along the lines of a *GW* (Green's function with Coulomb screening)-like approach<sup>33</sup> for interband transitions and supercell total energy calculations for localized transitions; and (iii) the evaluation of absorption and reflection spectra requires the explicit calculation of the complex dielectric function. All of the above listed points are, at least in principle, solved. For example, a simulated annealing total-energy technique would be able to predict stable structures, *GW* techniques have been demonstrated for semiconductors,<sup>33</sup> and the calculation of optical matrix elements has already been successfully demonstrated for a number of solid-state systems, for example, in the context of magneto-optics.<sup>34</sup> However, complex structures such as doped cerium sulfides with a combination of itinerant and localized phenomena still represent a substantial theoretical and computational challenge and intense efforts are required to refine the tools and approaches used in the present work.

Furthermore, despite the successes of theoretical and computational approaches to describe the complex electronic structure of compounds such as Na-doped  $\gamma$ -Ce<sub>2</sub>S<sub>3</sub>, one should keep in mind that the perceived color of a compound

involves a wealth of different intrinsic as well as extrinsic effects, such as particle size and surface effects, that are not amenable to a quantitative theoretical description. Thus the close dialog between the experimentalists and theoreticians is crucial to ensure a deeper understanding of the complexity of optical excitations upon which it should be possible to design and develop novel compounds with superior performance, better environmental compatibility, and more cost-effective synthesis routes.

## ACKNOWLEDGMENTS

The authors gratefully acknowledge fruitful discussions, especially with D. Huguenin, P. Macaudière, P. Maestro, A. Seigneurin (Rhône-Poulenc), J. Kübler (Technische Hochschule Darmstadt), and J. Sticht (MSI, San Diego), and M.-L. Theye, J. Lafait, and C. Witz (Université of Paris VI) for communicating their experimental results prior to publication. The crystal structures have been provided to us from the group of Professor Rouxel at the Institut des Matériaux de Nantes, which is gratefully acknowledged. We thank D. D. Koelling for suggesting a sensitivity test within atomic model calculations.

- 
- <sup>1</sup>P. Maestro, E.P. Patent No. 0203838 (30 April 1985).  
<sup>2</sup>T. Chopin, H. Guichon, and O. Touret, E.P. Patent No. 545746 (4 December 1991); P. Macaudière, E.P. Patent No. 680930 (6 May 1995).  
<sup>3</sup>G. Velleret and J. M. Tourre (unpublished).  
<sup>4</sup>E.-G. Scharmer, M. Leiß, and G. Huber, *J. Lumin.* **24/25**, 751 (1981).  
<sup>5</sup>V. P. Zhuze and A. I. Shelykh, *Fiz. Tekh. Poluprovodn.* **23**, 393 (1989) [*Sov. Phys. Semicond.* **23**, 245 (1989)].  
<sup>6</sup>V. A. Gubanov and M. V. Ryzhkov, *Zh. Strukt. Khim.* **27**, 123 (1986).  
<sup>7</sup>S. Kaciulis, A. Latisenka, and A. Plesanovas, *Surf. Sci.* **251/252**, 330 (1991).  
<sup>8</sup>S. Kimura, T. Suzuki, M. Ikezawa, and T. Kasuya, *Physica B* **186–188**, 387 (1993).  
<sup>9</sup>K. Takegahara, Y. Kaneta, and T. Kasuya, *J. Phys. Soc. Jpn.* **59**, 4394 (1990).  
<sup>10</sup>R. Dagys and G.-J. Babonas, *J. Solid State Chem.* **109**, 30 (1994).  
<sup>11</sup>G. Babonas, R. Dagys, and G. Pukinskas, *Phys. Status Solidi: B* **153**, 741 (1989).  
<sup>12</sup>R. Dagys, G.-J. Babonas, and G. Pukinskas, *Phys. Rev. B* **51**, 6995 (1995).  
<sup>13</sup>C. Witz, D. Huguenin, J. Lafait, S. Dupont, and M.-L. Theye, *J. Appl. Phys.* **79**, 2038 (1996) and (unpublished).  
<sup>14</sup>R. Mauricot, P. Gressier, M. Evain, and R. Brec, *J. Alloys Compounds* **223**, 130 (1995).  
<sup>15</sup>T. Suzuki *et al.*, in *Proceedings of the International Symposium on High Field Magnetism, Osaka, 1982*, edited by M. Date, (North-Holland, Amsterdam, 1983), p. 183.  
<sup>16</sup>W. H. Zachariasen, *Acta Crystallogr.* **2**, 57 (1949).  
<sup>17</sup>M. Picon, L. Domange, J. Flahaut, M. Guittard, and M. Patrie, *Bull. Soc. Chim. Fr.* **8**, 221 (1960).  
<sup>18</sup>P. Hohenberg and W. Kohn, *Phys. Rev. B* **136**, 864 (1964); W. Kohn and L. J. Sham, *Phys. Rev. A* **140**, 1133 (1965).  
<sup>19</sup>W. E. Pickett, A. J. Freeman, and D. D. Koelling, *Phys. Rev. B* **23**, 1266 (1981).  
<sup>20</sup>D. D. Koelling, A. M. Boring, and J. H. Wood, *Solid State Commun.* **47**, 227 (1983).  
<sup>21</sup>R. Podloucky and D. Glötzel, *Phys. Rev. B* **27**, 3390 (1983).  
<sup>22</sup>E. Wuilloud, B. Delley, W.-D. Schneider, and Y. Baer, *Phys. Rev. Lett.* **53**, 202 (1984).  
<sup>23</sup>M. R. Norman, E. Wimmer, and A. J. Freeman, *Phys. Rev. B* **32**, 7830 (1985).  
<sup>24</sup>R. Schumann, M. Richter, L. Steinbeck, and H. Eschrig, *Phys. Rev. B* **52**, 8801 (1995).  
<sup>25</sup>L. Hedin and B. I. Lundqvist, *J. Phys. C* **4**, 2064 (1971).  
<sup>26</sup>A. R. Williams, J. Kübler, and J. R. Gelatt, *Phys. Rev. B* **19**, 6094 (1979).  
<sup>27</sup>ESOCs User guide, 1995, MSI, San Diego, CA.  
<sup>28</sup>D. D. Koelling and B. N. Harmon, *J. Phys. C* **10**, 3107 (1977).  
<sup>29</sup>O. K. Andersen, *Phys. Rev. B* **12**, 3060 (1975).  
<sup>30</sup>The relativistic atomic program used here is based on routines by D. D. Koelling and B. Harmon (unpublished).  
<sup>31</sup>J. C. Slater, *Quantum Theory of Molecules and Solids* (McGraw-Hill, New York, 1974), Vol. 4.  
<sup>32</sup>P. Macaudière (private communication).  
<sup>33</sup>M. S. Hybertsen and S. G. Louie, *Phys. Rev. Lett.* **58**, 1551 (1987).  
<sup>34</sup>P. M. Oppeneer, T. Maurer, J. Sticht, and J. Kübler, *Phys. Rev. B* **45**, 10 924 (1992).